JMEPEG (2019) 28:852–862
https://doi.org/10.1007/s11665-018-3849-x

©ASM International
1059-9495/$19.00

Corrosion Inhibition Study of Mg-Nd-Y High Strength Magnesium Alloy Using Organic Inhibitor

G.R. Argade, S. Sanders, G. Mohandass, A. Alsaleh, F. D'Souza, T.D. Golden, and R.S. Mishra

(Submitted April 27, 2018; in revised form October 24, 2018; published online January 4, 2019)

A study on corrosion inhibition mechanism has been performed on rare earth containing WE43 magnesium alloy in 3.5 wt.% NaCl containing 8-hydroxyquinoline (HQ). After an initial increase in corrosion rate due to the formation of sparingly soluble MgQ_2 complex, it was found to decrease owing to inhibition effect of the complex. Scanning electrochemical microscopic analysis showed a decrease in corrosion currents and enhanced resistance to pitting corrosion was observed for WE43 samples in the presence of HQ after an exposure of 48 h. With time, the MgQ_2 thus generated formed a protective layer on the Mg alloy surface to prevent further corrosion. The corrosion rate of WE43 samples decreased by ~ 50% in HQ containing medium after a constant exposure of 28 days (from ~ 0.22 mg/cm^2 day in no HQ to ~ 0.11 mg/cm^2 day in HQ). For the WE43 samples in the presence of HQ, formation of MgO and MgQ_2 was detected by x-ray photoelectron spectroscopy and x-ray diffraction. Shallower and smaller pits appeared on the magnesium alloy with HQ in the solution as compared to deeper and larger pits on the samples with no HQ in the solution. The significance of metal-complexing organic agent, hydroxyquinoline, in initial acceleration and subsequent prevention of Mg corrosion via protective MgQ_2 complex layer formation is demonstrated.

Keywords corrosion inhibitor, magnesium alloy, scanning electrochemical microscopy, scanning electron microscopy, x-ray photoelectron spectroscopy

1. Introduction

During the past few years, corrosion susceptibility for magnesium and its alloys has received considerable attention from researchers due to their beneficial lightweight applications in aeronautics and automotive industries (Ref 1-3). In a recent review, Esmaily et al. (Ref 4) concluded that tailoring the surface properties of magnesium alloys through coatings or inhibitors was a reliable strategy for improvement in corrosion behavior. Previous efforts in this direction include the use of inorganic as well as organic compounds as inhibitors (Ref 5-9). Most of such corrosion inhibition studies were conducted on either pure magnesium or conventional AZ series alloys (Ref 5, 10-15). Very few studies were on rare-earth (RE)-added magnesium alloys (Ref 9, 16). These studies were carried out on Mg-Gd-Y alloy in ethylene glycol after exposure to multiple inorganic and organic compounds (Ref 9) and in ASTM D1384-87 (148 g/L Na_2SO_4 + 138 g/L $NaHCO_3$ + 165 g/L NaCl) corrosion water at pH of 8.2 to study synergy between organic silicates with inorganic zinc salt (Ref 16).

G.R. Argade and **R.S. Mishra**, Department of Materials Science and Engineering, University of North Texas, Denton, TX 76207; and Advanced Materials and Manufacturing Processes Institute, University of North Texas, Denton, TX 76203; **S. Sanders, G. Mohandass, A. Alsaleh, F. D'Souza,** and **T.D. Golden**, Department of Chemistry, University of North Texas, Denton, TX 76201; and Advanced Materials and Manufacturing Processes Institute, University of North Texas, Denton, TX 76203. Contact e-mail: GauravArgade@outlook.com.

It has been reported in the literature that 8-hydroxyquinoline (HQ) complexes with magnesium and forms a MgQ_2 complex (Ref 12, 13). There have been studies on corrosion inhibition using HQ on AZ91D magnesium alloys as a chemical conversion coating (Ref 13, 14). A combinatorial effect of HQ with sodium dodecylbenzenesulfonate has also been studied and reported to have higher efficiency due to a synergistic inhibition effect (Ref 12). Some work has also been reported on the behavior of an environmentally friendly corrosion inhibitor for WE43, a rare-earth-added magnesium alloy (Ref 17). RE-added magnesium alloys are attractive from a strength perspective due to their precipitation hardening capability, and no systematic study has been reported on influence of HQ on their corrosion mechanisms. With this focus, the present work is addressed toward exploring the corrosion mechanism of WE43 with exposure to 8-hydroxyquinoline. As demonstrated here using a variety of electrochemical and imaging techniques, the presence of HQ in fact accelerates the initial corrosion rate due to the formation of a MgQ_2 complex. However, the sparingly soluble MgQ_2 (K_{sp} = 6.8×10^{-12} mol/L) (Ref 18) forms a protective layer on the alloy surface to prevent further corrosion. The corrosion behavior is probed using constant immersion and electrochemical techniques in 3.5 wt.% NaCl solution with and without addition of HQ.

2. Experimental Section

2.1 Microstructure and Mechanical Properties

Hot-rolled Mg-Y-RE (4 wt.% Y, 3 wt.% Nd, 0.5% Zr and Mg balance: Mg-4Y-3Nd) alloy was used as the substrate for all experiments, henceforth designated as WE43. Microstructural characterization was done using FEI Quanta 200 environmental scanning electron microscope (ESEM). Mechanical properties were assessed using microhardness and uniaxial tensile testing

in transverse orientation to the rolling direction. Microhardness was performed on a Wilson hardness tester with a 300-g load, and tensile testing was performed on a custom built tensile tester.

2.2 Corrosion Measurements

Constant immersion tests were conducted in 3.5 wt.% NaCl and 3.5 wt.% NaCl + 3.8 mM HQ solutions at room temperature. The electrochemical measurements were conducted using same electrolyte conditions with (1) potentiodynamic polarization, (2) electrochemical impedance spectroscopy (EIS), and (3) galvanostatic and potentiostatic polarization. All the samples were ground and polished through 1200-grit paper and subsequently cleaned in ethanol before conducting any corrosion tests. For immersion tests, samples were studied for 7-, 14-, and 28-day exposure with and without HQ. Three samples for each condition were employed to incorporate statistical variation. Similarly, all the electrochemical studies were conducted at least three times to check for repeatability of results. Surface area and initial weight measurements (with accuracy of 0.0001 g) were taken for all the samples before exposing them to immersion testing. At the end of immersion tests, the respective samples were cleaned by immersing them in hot 15% chromic acid solution to dissolve the corrosion products from the surface, immediately followed by cleaning with acetone. Final weight of the samples was measured to calculate corrosion rate. Cleaned samples were observed under FEI Quanta ESEM to characterize the surface corrosion. For electrochemical measurements, samples were allowed to equilibrate for one hour at open-circuit potential (OCP) before conducting any potentiodynamic polarization or EIS scans. Potentiodynamic polarization scans were run at t_0 (immediately after 1 h OCP in 3.5 wt.% NaCl) and t_{48} (sample exposed to 48 h in 3.5 wt.% NaCl) at a scan rate of 0.166 mV/s. The potential sweep was initiated from cathodic direction moving toward anodic direction. EIS scans were made from 10 kHz to 10 mHz frequency range for the t_0 and t_{48} samples. For galvanostatic study, constant current density of 0.1 mA/cm^2 was applied throughout the 24-h electrolysis period. The selection of current density was on the basis of polarization plots. The current density was selected so as to be in the breakdown region to induce pitting corrosion and measure subsequent potentials. Similarly, for potentiostatic polarization, a potential of − 1625 mV versus SCE was applied for electrolysis duration of 24 h. Again, this selection was also on the basis of polarization plots. Linear polarization resistance was measured for WE43 samples under no-HQ and HQ-added conditions in 3.5 wt.% NaCl solution as a function of time. The potentials were scanned ± 20 mV versus OCP starting from cathodic to anodic directions for measurements of linear polarization resistance. The samples were held at OCP for 1 h before conducting the linear polarization resistance tests. For all the electrochemical measurements, saturated calomel electrode (SCE) was used as the reference electrode and platinum as the counter electrode. All the measurements were taken at room temperature. Electrochemical measurements were taken using a Parstat 4000 potentiostat.

Scanning electrochemical microscopy (SECM) was performed using an Ametek VersaScan Electrochemical Microscope. A platinum ultramicroelectrode (UME) tip having 25 μm diameter, saturated Ag/AgCl, and platinum wire were used as the working, reference, and counter electrodes, respectively. Considering the conductivity of the solution, the chloride concentration was reduced and the WE43 samples were exposed to 0.5 wt.% NaCl solution with and without HQ. The platinum UME was biased at 0.1 V versus saturated Ag/AgCl in order to measure any H_2 gas produced at the magnesium surface as a result of corrosion activity. A similar approach was used to record the H_2 production via SECM on a Mg substrate by Salleh et al. (Ref 19). An SECM image in constant height mode was obtained by scanning the UME tip in the *x*–*y* plane and recording the tip current as a function of tip location. The distance between tip and substrate was adjusted to 25 μm by performing an approach curve using ferrocenemethanol as a redox mediator, holding the probe potential at a value of 0.6 V to oxidize the ferrocenemethanol in solution. After the approach curve was completed, the redox mediator solution was removed and the sample was washed carefully. The 0.5% NaCl solution was then added to the cell to perform the SECM analysis with and without HQ. All samples for SECM analysis were mirror polished using 1-μm diamond paste in ethanol environment. An area surrounding the WE43 sample (mounted in epoxy) was examined to differentiate tip current as compared to the area directly over the magnesium sample. All SECM measurements were taken at room temperature.

2.3 Corrosion Product Analysis

After testing, surface characterization of the samples was conducted using SEM. Corrosion product analysis was performed with x-ray diffraction (XRD) and x-ray photoelectron spectroscopy (XPS) for all the WE43 samples. The XPS was performed using a PHI 5000 VersaProbe II spectrometer with an Al K-α x-ray source, and the spectra were recorded for Mg—2*p*, O—1*s*, and Nd—3*d*5. Peak calibration was done using C—1*s* spectrum peak at 284.6 eV. XRD was performed using a Rigaku Ultima III with a Cu Kα source at 40 kV accelerating voltage and 44 mA current at a 0.05° step size and 3°/min scan rate. The magnesium–HQ complex formed has fluorescent characteristics, so fluorescence microscopy was conducted to observe the surface of HQ-added WE43 samples as a function of time. A Nikon Eclipse Ti microscope was used by flashing ultraviolet light on the WE43 sample surface to capture the fluorescent micrographs.

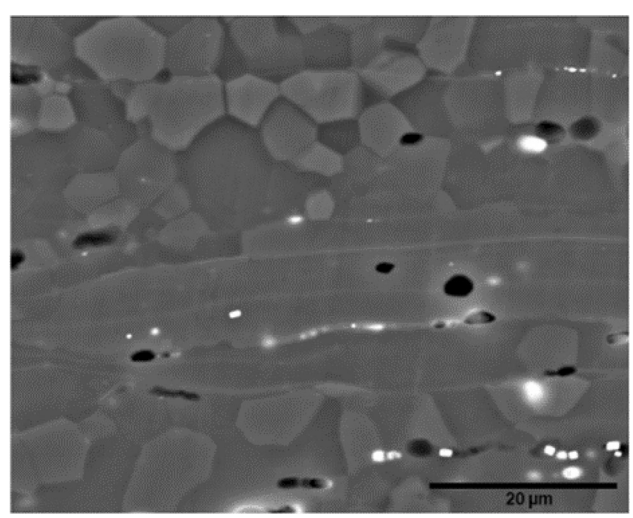

Fig. 1 Scanning electron micrograph of WE43 sample

Table 1 Results of mechanical testing of WE43 alloy

Microhardness, HV300	Yield strength, MPa	Tensile strength, MPa	Elongation, %
81.5 ± 1.5	182.3 ± 2.1	253 ± 9.8	22.3 ± 5.5

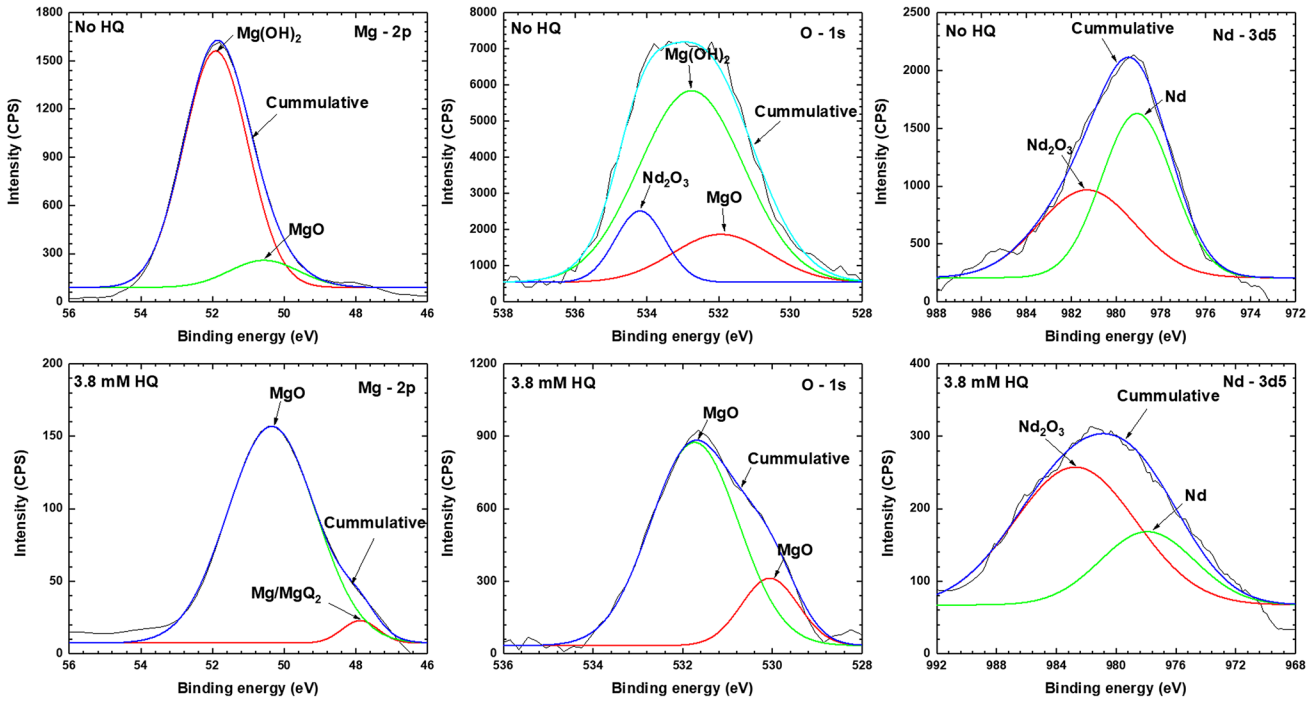

Fig. 2 Results of XPS analysis of WE43 samples after 48-h exposure in 3.5 wt.% NaCl and 3.5 wt.% NaCl + 3.8 mM HQ solutions

3. Results and Discussion

The following section describes the results of corrosion product analysis and electrochemical measurements taken on WE43 alloy samples in 3.5 wt.% NaCl solution and 3.5 wt.% NaCl solution + 3.8 mM HQ solution at room temperature. Comparison is made between initial exposed samples with samples exposed to these conditions for 48 h of duration.

3.1 Microstructure and Mechanical Properties of WE43 Alloy

Initial microstructural characterization of the as-received WE43 alloy was conducted using acetic picral as etchant. SEM micrograph of the alloy is shown in Fig. 1. The microstructure consists of equiaxed and elongated grains in the rolling direction with Y- and Nd-rich bright particles in the matrix. Microhardness testing with 300 g load and tensile testing were conducted to evaluate the mechanical properties of the alloy. Results of microhardness and tensile testing are summarized in Table 1. For microhardness, an average of ten measurements was reported and for tensile testing three WE43 samples were tested. The alloy showed microhardness, yield strength, ultimate tensile strength, and ductility of 81.5 HV, 182.3 MPa, 253 MPa, and 22.3%, respectively. These values were consistent with those reported by Panigrahi et al. (Ref 20).

3.2 Corrosion Product Analysis of WE43 Alloy

The XPS spectra recorded from WE43 samples exposed to 3.5 wt.% NaCl with and without 3.8 mM HQ after 48-h exposure in respective solutions are shown in Fig. 2. A clear change in composition of corrosion product was observed. For Mg—2*p* spectrum, the samples without HQ in the solution showed predominantly $Mg(OH)_2$ (a large peak at 51.9 eV) with small fraction of MgO (peak at 50.5 eV). On the other hand, samples with HQ in the solution showed mainly the MgO peak with a small peak possibly associated with MgQ_2 (a lower binding energy peak at 47.9 eV). Similarly, for O—1*s* spectrum, no-HQ condition depicted mostly $Mg(OH)_2$, with some Nd_2O_3 and MgO, whereas the sample with HQ in the solution showed only MgO peak. Pinto et al. (Ref 21) and Ardelean et al. (Ref 22) reported similar binding energy values for $Mg(OH)_2$ and MgO for Mg—2*p* and O—1*s*. In a recent review on corrosion inhibitors for magnesium alloys, a suggestion was made about suppression of anodic dissolution as a possible mechanism of corrosion inhibition by HQ (Ref 23). In this study, there was clear indication by XPS about the formation of MgQ_2 and MgO in the top most layer of corrosion products that provided the corrosion protection. This protective layer reduced further anodic dissolution of Mg and improved corrosion resistance. The absence of $Mg(OH)_2$ in the top most layer of corrosion products in the presence of HQ enhanced the corrosion resistance of WE43. The Nd—3*d*5 peaks of neodymium were observed for both no-HQ and HQ solutions.

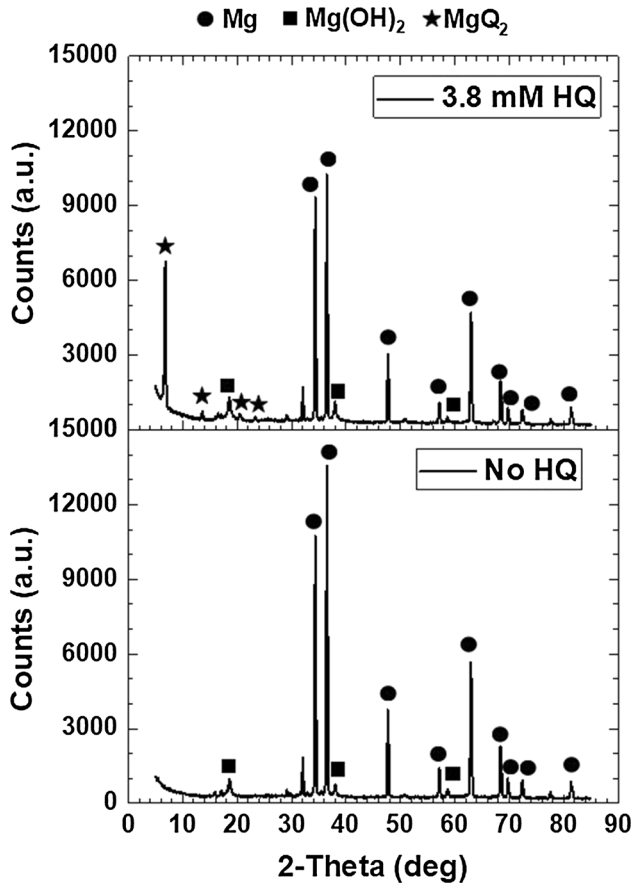

Fig. 3 XRD analysis of WE43 samples after 48-h exposure in 3.5 wt.% NaCl and 3.5 wt.% NaCl + 3.8 mM HQ solutions

The XRD results in Fig. 3 corroborated the XPS analysis. MgQ_2 peaks were detected in the XRD analysis of the sample exposed to 3.5 wt.% NaCl with 3.8 mM HQ. In a study conducted by Kartsonakis et al. (Ref 8) on corrosion inhibition of ZK30 magnesium alloy, similar peaks were detected in XRD attributed to a MgQ_2 complex. Shen et al. (Ref 14) observed MgQ_2 peaks on the AZ91D magnesium alloy coated with 8-hydroxyquinoline primer. Thus, it is evident that the peaks observed in the range of 12°-25° 2-theta values correspond to formation of MgQ_2 complex for WE43 samples exposed to HQ-added solution.

3.3 Constant Immersion and Electrochemical Measurements

The results of constant immersion, potentiodynamic polarization, galvanostatic, and potentiostatic polarization of WE43 samples in 3.5 wt.% NaCl and 3.5 wt.% NaCl + 3.8 mM HQ solutions are presented in Fig. 4. Constant immersion tests (Fig. 4a) showed a decrease in corrosion rates for samples exposed to solution with HQ. The samples exposed to solution with HQ after 28 days showed ~ 50% lower corrosion rates than samples without HQ in the solution. The corrosion rates were calculated through weight loss measurements before and after exposure. The constant immersion tests showed amplification in the corrosion inhibition with longer exposure durations (lower weight loss for 28-day exposed sample as compared to 14 days). From the weight loss analysis through constant immersion tests, it is evident that the corrosion inhibition efficiency (C.I.) calculated as shown in Eq 1 had an increasing trend with exposure time. C.I. after 7 days of exposure was ~ 26% which increased to 40% after 14 days of exposure. For the 28-day exposure, C.I. further increased to 50% (see Fig. 4a).

$$\%\text{C.I.} = 100 \times (\text{C.R.}_{\text{without HQ}} - \text{C.R.}_{\text{with HQ}})/\text{C.R.}_{\text{without HQ}}. \quad \text{(Eq 1)}$$

where C.R. is the corrosion rate.

Potentiodynamic polarization scans in Fig. 4(b) showed large passive range for samples exposed to solution without HQ after 48-h exposure; however, the samples in the presence of HQ after an exposure of 48 h showed lower corrosion currents with marginally positive corrosion potentials. The electrochemical parameters from potentiodynamic polarization are summarized in Table 2. The differences in the corrosion behavior studied through constant immersion as compared to the electrochemical measurements are well known in magnesium alloys owing to the negative difference effect (NDE) where with an increase in potential the hydrogen evolution rate increases along with higher corrosion (Ref 24, 25). More positive corrosion potentials with lower corrosion currents were observed for samples exposed to HQ-added solution after 48 h. Shorter times to reach stable potentials and lower currents were observed for samples in the presence of HQ, as shown in Fig. 4(c) and (d) for galvanostatic and potentiostatic polarization, respectively. These samples reached a stable potential within ~ 8 h of 0.1 mA galvanostatic measurements, whereas the samples exposed to solution with no HQ reached a stable potential in ~ 16 h. Under potentiostatic conditions, the samples exposed to solution with HQ demonstrated lower current (~ 2 ×) as compared to those with no HQ in the solution throughout the 24-h duration of the test. The selection of current density for galvanostatic measurements and that of voltage for potentiostatic measurements were based on the polarization plots. These were selected to impress accelerated corrosion conditions to assess the behavior. The galvanostatic and potentiostatic results indicated the reduction in corrosion behavior of the magnesium alloy in the presence of HQ. To further emphasize this effect, linear polarization resistance (R_p) was measured as a function of time for WE43 samples exposed to 3.5 wt.% NaCl with and without HQ. The WE43 samples exposed to solution with HQ showed ~ sixfold increase in the polarization resistance after 48 h of exposure. On the other hand, for the samples without HQ in the solution exposed for same duration of 48 h, there was ~ 13% increase in polarization resistance. The polarization resistance values are listed in Table 2. The linear polarization resistance values for the WE43 in 3.5 wt.% NaCl solution were a good match with the reported values for identical conditions (Ref 26).

Electrochemical impedance spectroscopy (EIS) results with Nyquist and Bode magnitude plots are shown in Fig. 5(a) and (b), respectively, for WE43 in 3.5 wt.% NaCl with and without HQ taken immediately after immersion (t_0) and after 48 h of immersion in solution (t_{48}). These samples showed two capacitive loops: one each at high and low frequencies. The high-frequency capacitive loop is attributed to charge transfer, whereas the lower-frequency one is attributed to the mass transport across the surface corrosion layer (Ref 12, 22, 26, 27). The equivalent circuits for samples exposed to with and without HQ in the solution are presented in Fig. 5(c) and (d), respectively. Due to the depressed nature of the semicircles as

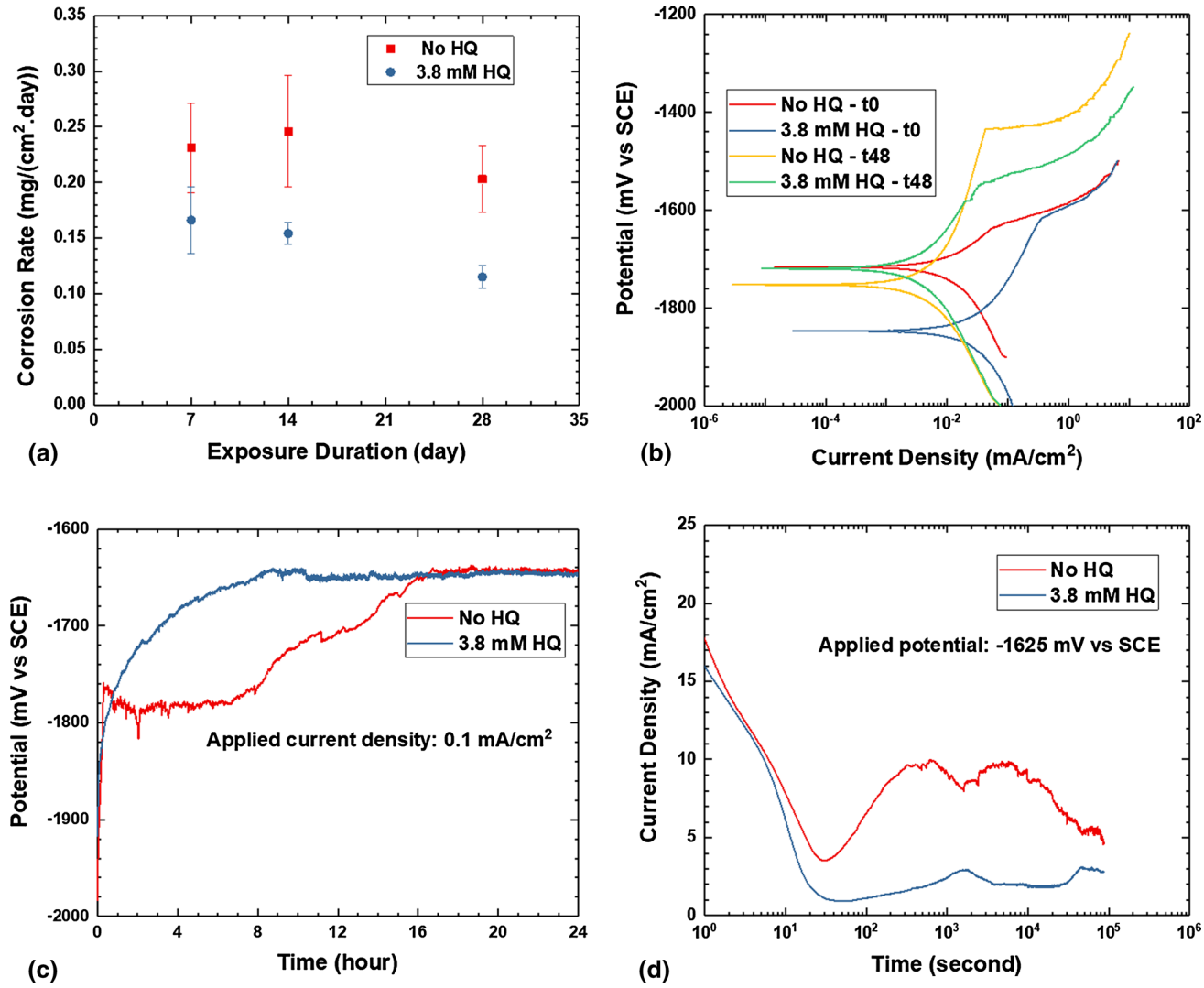

Fig. 4 (a) Constant immersion testing, (b) potentiodynamic polarization plots, (c) galvanostatic plots, (d) potentiostatic plots of WE43 alloy in 3.5 wt.% NaCl with and without HQ

Table 2 Electrochemical parameters from the polarization plots of WE43 samples exposed to in 3.5 wt.% NaCl with and without HQ

Condition	E_{corr}, mV vs. SCE	i_{corr}, μA/cm^2	Linear polarization resistance, Ω cm^2
WE43—no HQ t_0	− 1717	1.76	2283 ± 437
WE43—no HQ t_{48}	− 1752	0.6	4087 ± 127
WE43—3.8 mM HQ t_0	− 1846	3.25	736 ± 187
WE43—3.8 mM HQ t_{48}	− 1718	0.4	4646 ± 210

evident in the Nyquist plots, constant phase elements (CPEs) were used instead of the ideal capacitors. This is typically observed for solid electrodes to account for non-ideal behavior. In the equivalent circuits, R_{sol} corresponds to the solution resistance between the working electrode and reference electrode. For the samples without HQ in the solution, the equivalent circuit has a constant phase element CPE_{ox} (related capacitance of oxide film) and associated oxide film resistance (R_{ox}). Further, the circuit has another CPE_{dl} which is associated with the capacitance of the double layer and R_{ct}, the resistance of charge transfer at the metal interface. For the samples with HQ in the solution, the first CPE has been modified to reflect the formation of a corrosion inhibition layer, MgQ_2, rather than an oxide layer. This replacement is justified based upon the lower intensity of the MgO peak in the O—1*s* XPS spectrum shown in Fig. 2. Additionally, the resistance has been changed to the resistance of the layer formed from the HQ adsorbed to the metal surface (Ref 8). The fitting of EIS data was carried out using ZView 2 software. The results of EIS data analysis are summarized in Table 3. A good fit for the Nyquist and Bode plots was achieved using these electrical circuits for individual conditions, and fitted plots are shown in Fig. 5(a) and (b). For

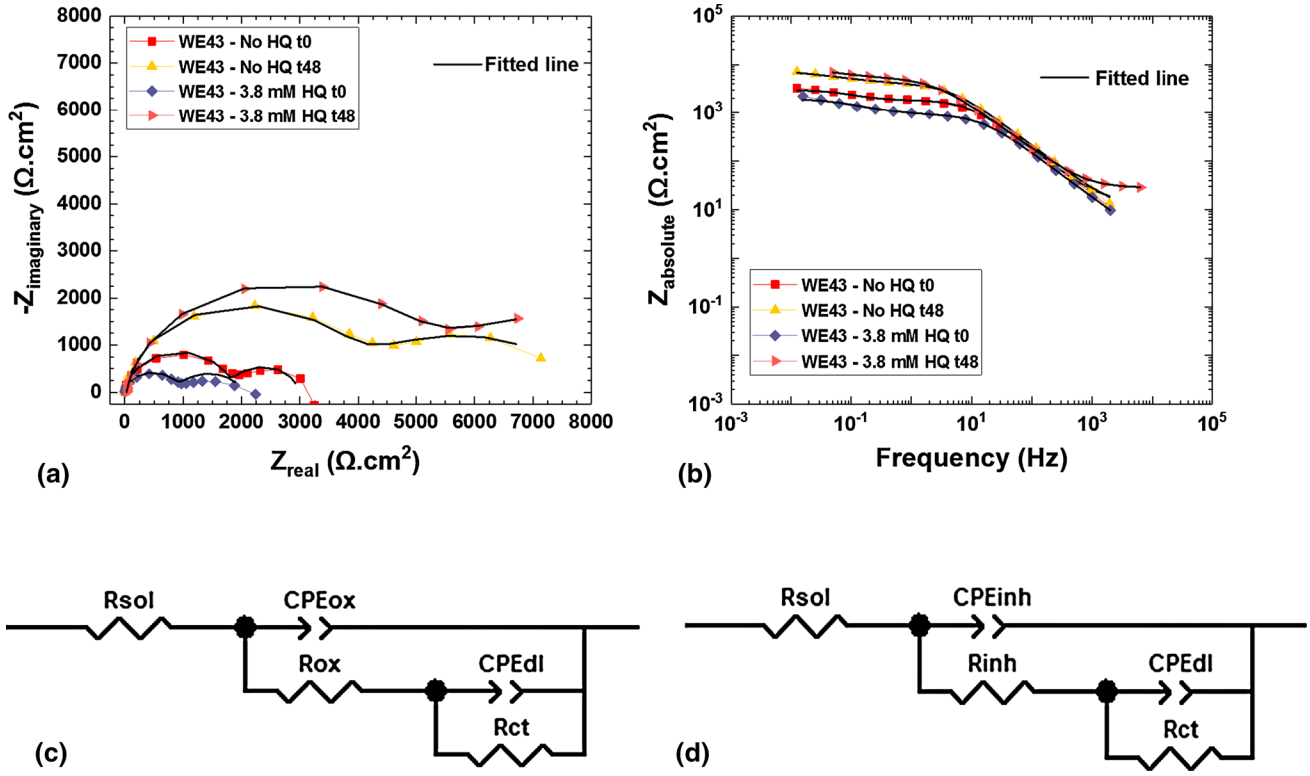

Fig. 5 (a) Nyquist plots, (b) Bode plots and equivalent circuits for (c) samples without HQ in the solution and (d) in the presence of HQ in 3.5 wt.% NaCl solutions

Table 3 Summary of the values of equivalent circuit elements obtained after fitting the EIS data of WE43 samples with and without HQ in 3.5 wt.% NaCl solutions

Condition	$CPE_{ox} - T$, F cm^{-2} s^{-n}	n_{ox}	R_{ox}, Ω cm^2	$CPE_{inh} - T$, F cm^{-2} s^{-n}	n_{inh}	R_{inh}, Ω cm^2	$CPE_{dl} - T$, F cm^{-2} s^{-n}	n_{dl}	R_{ct}, Ω cm^2	R_p, Ω cm^2
WE43—no HQ t0	1.1×10^{-5}	0.95	1826	…	…	…	1.5×10^{-3}	0.92	1136	2962
WE43—no HQ t48	1.1×10^{-5}	0.93	3943	…	…	…	6.8×10^{-4}	0.64	4002	7945
WE43—3.8 mM HQ t0	…	…	…	1.6×10^{-5}	0.93	920	1.3×10^{-3}	0.76	1102	2022
WE43—3.8 mM HQ t48	…	…	…	1.6×10^{-5}	0.90	5181	7.3×10^{-4}	0.64	5514	10,695

the samples in the presence of HQ, an increase in inhibition layer resistance (R_{inh}) and charge transfer resistance (R_{ct}) with corresponding marginal decrease in respective capacitances was observed with an increase in time. The plots also indicate that early on (at t_0), the sample without HQ in the solution has larger capacitive loops as compared to the one with HQ. However, the samples exposed to solution with HQ after 48-h duration showed larger loops, indicating higher corrosion resistance. The effect of inhibition was clearly observed with the marked increase in the two capacitive loop resistances. Figure 6 shows the plot of R_{ox}/R_{inh} and R_{ct} for WE43 samples, and there was a clear increase in the resistances of the samples exposed to solution with HQ after 48 h of duration. The polarization resistances for the WE43 samples can be estimated from the EIS analysis as described in Eq 2a and 2b, respectively (Ref 28, 29).

$$\frac{1}{R_p} = \frac{1}{R_{ox} + R_{ct}} \quad \text{(Eq 2a)}$$

$$\frac{1}{R_p} = \frac{1}{R_{inh} + R_{ct}} \quad \text{(Eq 2b)}$$

where R_p is the polarization resistance.

It is evident that the increase in the cumulative resistance values of samples exposed to HQ-added solution over the period provided higher corrosion resistance as compared to those without HQ. The polarization values as estimated from Eq 2a and 2b are also reported in Table 3. These polarization values showed similar trend as the linear polarization resistance presented in Table 2; however, the magnitudes were found to be higher in the EIS calculated values. The increase in R_{ct} and

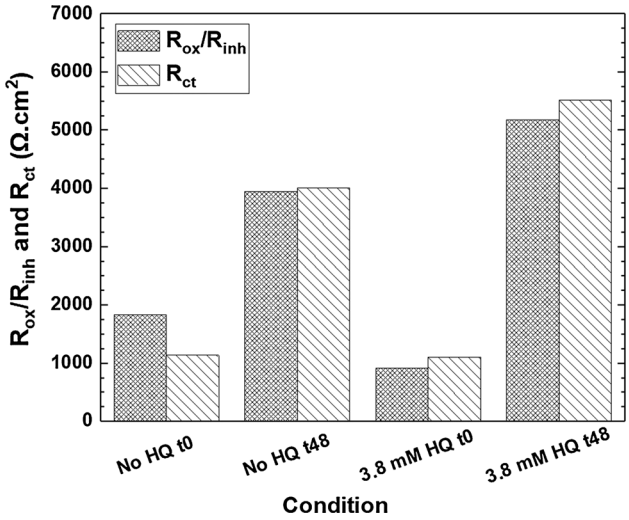

Fig. 6 Plot of fitting parameters of equivalent circuits of WE43 samples with and without HQ in 3.5 wt.% NaCl solutions

R_{ox} for samples in the absence of HQ in the solution for 48-h exposure can be attributed to $MgO/Mg(OH)_2$ layer formation on the surface. However, with time the protective ability of $MgO/Mg(OH)_2$ layer is expected to diminish as it is not stable. On the other hand, the samples exposed to solution with HQ showed the marked increase in the polarization resistances (both through LPR and EIS) with exposure time. The polarization resistance is expected to further increase with time (as observed in the constant immersion tests) based upon the increase in corrosion inhibition efficiency shown from weight loss analysis after 7, 14, and 28 days (Fig. 4a).

The SECM area scans with different local corrosion current characteristics of WE43 samples when magnesium is exposed to a 0.5 wt.% NaCl solution with and without HQ are shown in Fig. 7. For the sample without HQ in the solution, the t_0 profiles show relatively uniform corrosion with some regions showing higher current values as observed in Fig. 7(a). The behavior after an exposure of 48 h of the same sample illustrated in Fig. 7(b) showed a large area with low levels of currents, whereas a very small area showed relatively higher current values. This suggests that the sample without HQ in the solution after 48 h of exposure passivated likely under the formation of $Mg(OH)_2$ film on the surface. However, localized corrosion observed on the surface due to lack of passivity of the film is evident from the higher current values in a highly localized region. On the other hand, WE43 sample in the presence of HQ in the solution at t_0 (see Fig. 7c) largely showed higher currents all throughout the sample surface when compared with sample with no HQ in the solution t_0 (see Fig. 7a) condition. A decrease in the currents was observed after 48 h of exposure. Magnesium alloys are known to undergo localized pitting corrosion in chloride containing aqueous solutions. For the RE-added alloys, second phase rich in RE acts as cathodic sites and creates a galvanic condition with the anodic Mg matrix (Ref 30). SECM mapping of Mg corrosion has difficulties using H_2 as the mediator. However, it can provide semiqualitative comparison about the corrosion occurring on the surface which is typically accompanied by H_2 evolution (Ref 19, 31). In the present study, the comparison was made between corrosion behavior of WE43 in chloride solution having no-HQ and HQ-added conditions over the period of 48-h exposure. The currents measured in the SECM analysis were only compared between t_0 and t_{48} of respective conditions (i.e., with HQ and without HQ) to evaluate the extent of corrosion. The WE43 samples without HQ in the solution showed localized spots of higher currents in the SECM analysis (see Fig. 7b) representing the pitting corrosion happening on the surface. On the other hand, as evident in Fig. 7(d) the current levels are suppressed across the sample surface owing to formation of protective MgQ_2 film. The film formed on the surface of the sample insulates it from further corrosion. On all the samples analyzed with SECM, approach curves were used to select an appropriate distance for the probe, as described in "Experimental" section. A representative approach curve is presented in Fig. 7(e). Thus, addition of HQ in the solution resulted in higher pitting corrosion resistance of WE43 alloy. However, as observed in the polarization results, the 48-h WE43 sample without HQ in the solution showed $\sim$ 80-100 mV positive pitting potential as compared to the one with HQ in the solution (see Table 2). This again highlights the difference of corrosion behavior in magnesium alloys under open-circuit and polarized conditions. The SECM analysis conducted in this work was in a open-circuit environment. Thus, these results provide a microscopic evidence of the corrosion inhibition mechanism of HQ for the magnesium alloy. Through SECM, it was evident from the lack of large local currents that addition of HQ provided WE43 a resistance to attack under pitting corrosion in chloride containing environments after prolonged exposure.

Since the MgQ_2 complex is luminescent (Ref 32), fluorescence microscopy images of the surface were recorded as a function of time to study the growth of the corrosion protective layer. Figure 8 shows the fluorescent micrographs of the WE43 samples in the presence of 3.8 mM HQ + 3.5 wt.% NaCl solution taken after 1, 24, and 48 h of exposure. Initially, the film was not continuous and therefore less protective (see Fig. 8a); however, with time the film grows uniformly and appeared to be compact (see Fig. 8b and c). The continuous nature of the film provided the corrosion protection with a decrease in corrosion activity. Scanning electron micrographs after 28-day exposure for the constant immersion samples are shown in Fig. 9(a) and (b). The sample with no HQ in the solution showed indiscriminate type of metal dissolution under pitting with spiral contours visible in the inset micrograph of Fig. 9(a). On the other hand, the sample HQ in the solution showed typical hemispherical pitting behavior (see inset Fig. 9b). Note that the grain structure of the alloy is observed in the pitted region. Also, note the larger pit sizes for the sample with no HQ in the solution compared to the smaller pits for the sample in the solution added with HQ.

The difference in the mechanism of corrosion inhibition of magnesium alloy through addition of HQ as compared to earlier reported results is explained below. As indicated in the electrochemical analyses, the corrosion activity increased in the initial period. This was attributed to the active dissolution of Mg due to the presence of Cl^- and HQ. The formation of a sparingly soluble MgQ_2 complex on the surface of sample exposed to HQ-added chloride solution was confirmed via XPS and XRD analysis. The sparingly soluble nature of this

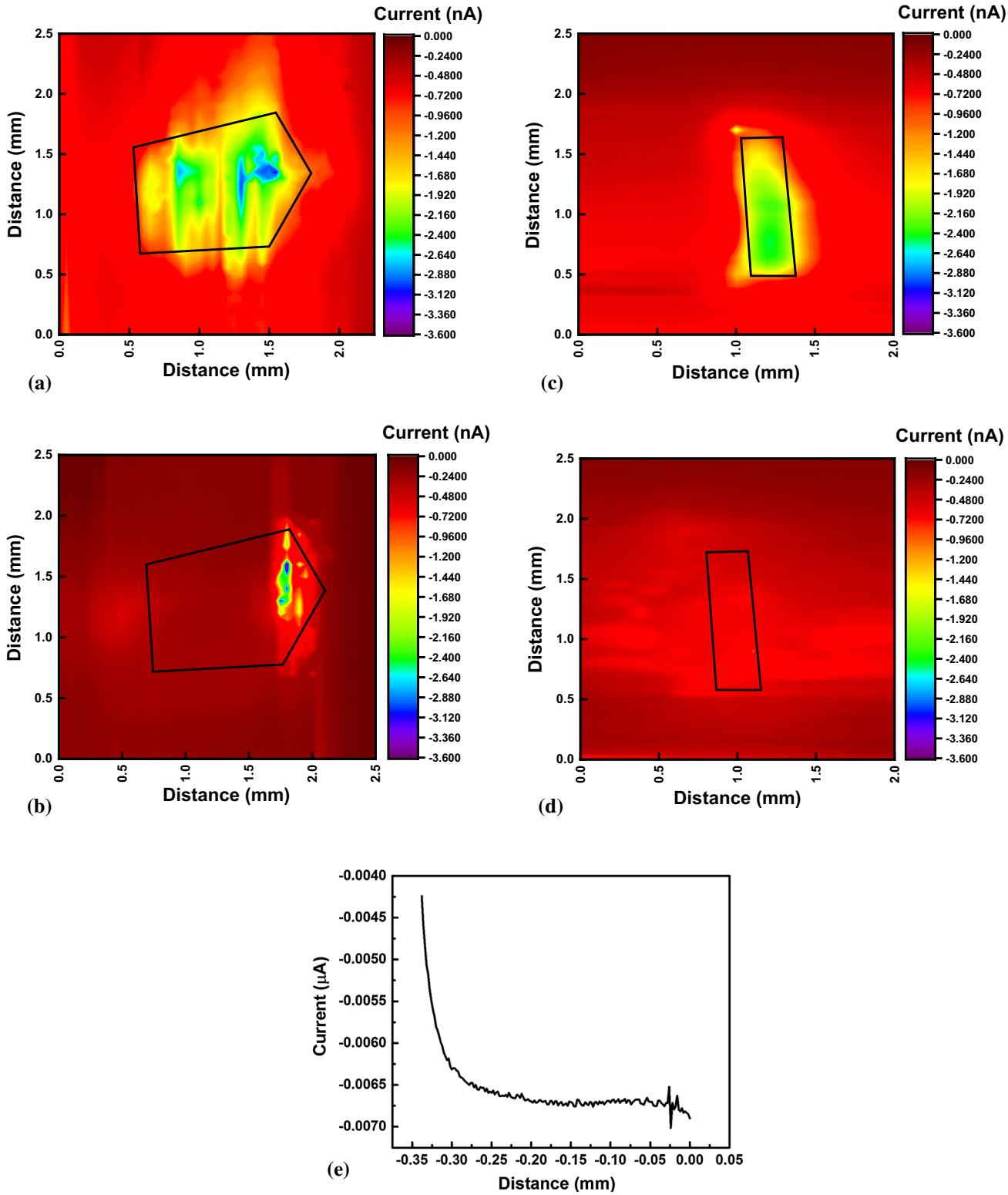

Fig. 7 Scanning electrochemical microscopy results of WE43 with no HQ (a and b) and HQ (c and d) added in 0.5 wt.% NaCl solution for time t_0 and t_{48}, respectively. A representative approach curve is shown in (e)

complex resulted in continuous and compact formation of a protective corrosion barrier on the Mg alloy surface.

Magnesium corrosion in aqueous environment is normally described as follows:

$$Mg \rightarrow Mg^{2+} + 2e^- \quad \text{(anodic reaction)} \qquad \text{(Eq 3)}$$

$$2H_2O + 2e^- \rightarrow 2OH^- + H_2 \quad \text{(cathodic reaction)} \qquad \text{(Eq 4)}$$

Thus, for samples with no HQ the overall reaction is:

$$Mg + 2H_2O \rightarrow Mg(OH)_2 + H_2 \qquad \text{(Eq 5)}$$

And for the samples in the presence of HQ in addition to Eq 5 there will be,

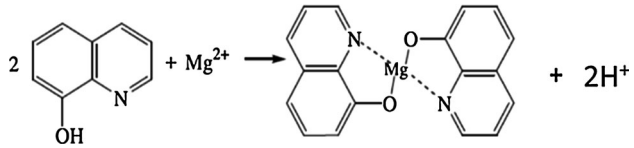

(Eq 6)

In this case, the reaction is between magnesium and HQ, wherein the Mg^{2+} ions produced from the anodic reaction combines with two molecules of hydroxyquinoline to generate a MgQ_2 complex as described above and the hydrogen ions generated can combine to evolve as hydrogen gas when the pH of the system reaches an equilibrium (Ref 13, 14).

In the presence of HQ, the magnesium ions generated as part of the anodic reaction combine to form a complex as illustrated in Eq 6 (Ref 13, 14). As this complex is formed, excess magnesium dissolution happens and additional hydrogen evolution takes place. For the SECM analysis, hydrogen evolution was taken as the basis for the current profiles observed on the samples. Thus, the t_0 sample with HQ in the solution showed higher current levels as depicted in Fig. 7(c). After 48 h of exposure, the formation of a complex on the sample surface led to negligible currents (see Fig. 7d). The effect of this layer was evident in the constant immersion as well as electrochemical measurements in HQ-added 3.5 wt.% NaCl solution.

In some studies (Ref 23), the corrosion inhibition efficiency with HQ for WE43 alloy was presented as negative. However, it is important to note that the action of corrosion inhibition with HQ initiates over time and this fact is emphasized in this study. The EIS results of samples in the presence of HQ in the solution are expected to show improving trends over time. The behavior is also anticipated from the literature (Ref 8, 12) wherein a monotonic increase in the corrosion resistance of Mg alloys was observed for HQ-added conditions with time. The difference between those studies and the present study is the concentration of the chloride species. As observed in the present study, the initial increase in the corrosion rates was predominantly responsible for different corrosive media employed as compared to those by Kartsonakis et al. (Ref 8) and Gao et al. (Ref 12). Thus, HQ with higher chloride concentration (0.6 M NaCl) initially increased Mg dissolution which resulted in stable formation of protective MgQ_2 layer as explained above. For magnesium alloys, corrosion behavior studied through electrochemical and constant immersion (open-circuit conditions) is typically carried out. In a recent studies, King et al. (Ref 28) and Shkirskiy et al. (Ref 29) bring out this

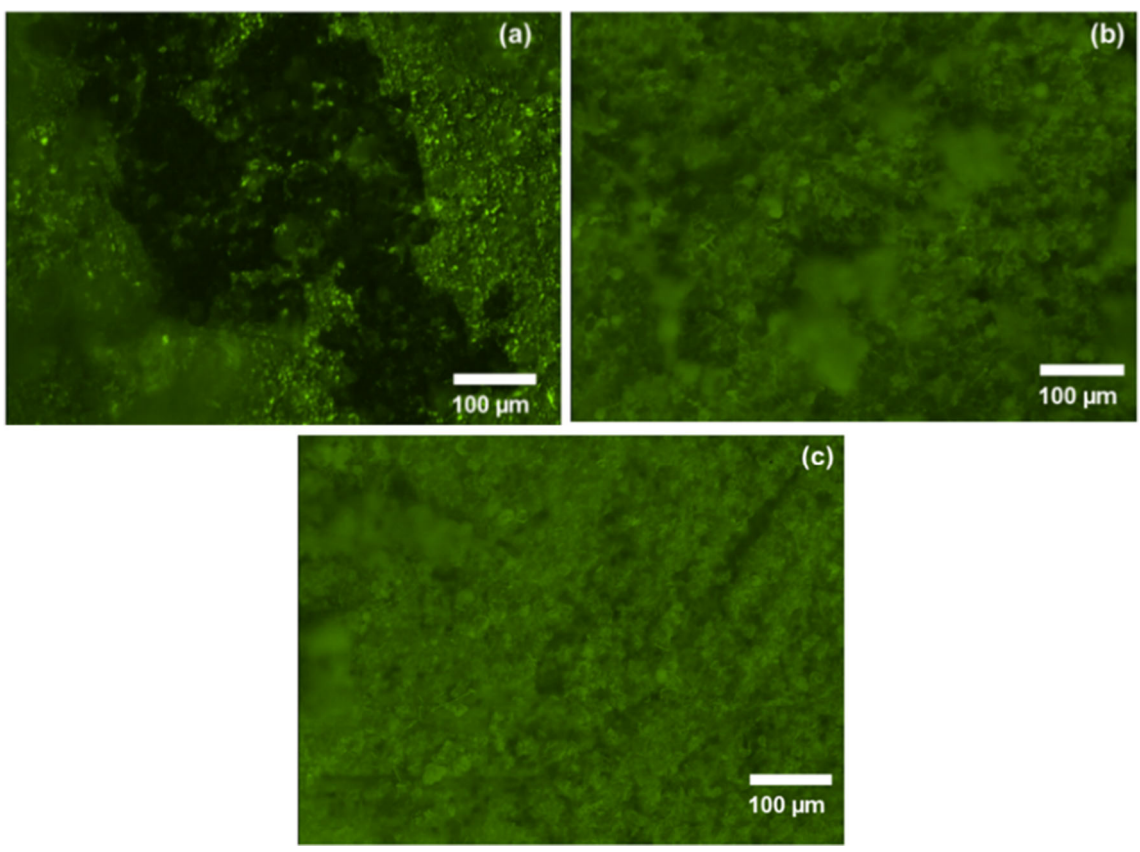

Fig. 8 Fluorescent micrographs of WE43 samples taken at (a) 1-h, (b) 24-h, and (c) 48-h exposure in 3.5 wt.% NaCl + 3.8 mM HQ solution

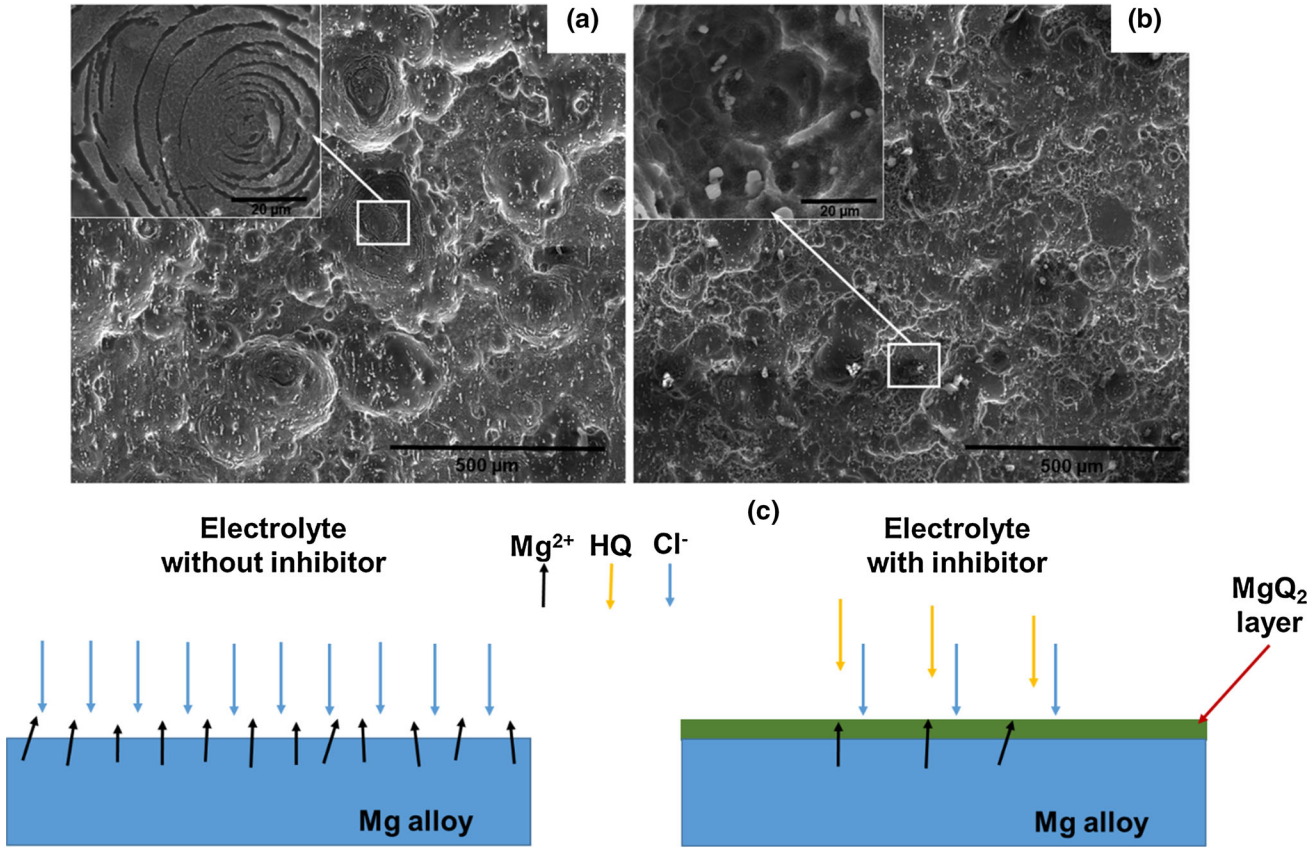

Fig. 9 Scanning electron micrographs of WE43 (a) no HQ and (b) 3.8 mM HQ after 28 days of exposure in 3.5 wt.% NaCl and (c) schematic of corrosion inhibition mechanism in the presence of HQ

fact by simultaneously employing EIS, mass loss, and hydrogen gas collection and EIS and atomic emission spectroelectrochemistry (AESEC), respectively, on pure magnesium in chloride environments. Thus, in this study the corrosion inhibition of WE43 was studied through various electrochemical techniques along with constant immersion. The results of both the techniques indicated similar trends of WE43 corrosion inhibition through HQ.

The lower corrosion currents and an increase in the polarization resistance for the sample exposed to HQ-added solution during SECM scans are attributed to the protective nature of this layer. Thus, through this study it became evident that the corrosion inhibition of WE43 magnesium alloy in the presence of HQ is realized with the increase in exposure time. After an initial drop in the corrosion resistance and subsequent formation of stable MgQ_2 layer, the corrosion activity was found to reduce. The sequence of events that happen in the presence of HQ can be explained as follows: (1) Initial corrosion activity leads to magnesium dissolution, (2) HQ binds with magnesium to form MgQ_2 layer, (3) growth of this layer, and (4) barrier to restrict further interaction with Cl^- ions. Once the optimum thickness of the MgQ_2 layer is achieved, further corrosion activity is impeded. The insoluble nature of this layer adds to the stability and thus helps in providing enhanced corrosion inhibition. A schematic of the process of corrosion inhibition achieved through HQ is described in Fig. 9(c). To further enhance the corrosion inhibition, in addition to optimization of HQ concentration, a modification of HQ structure by synthesizing long alkyl chains will be undertaken. This will also provide key insights into the corrosion inhibition process and corrosion monitoring of magnesium alloys using HQ.

4. Conclusions

Corrosion inhibition of WE43 with 8-hydroxyquinoline was studied in 3.5 wt.% NaCl solution. It was observed that in the presence of HQ, the corrosion resistance initially dropped; however, it increased upon formation of a stable MgQ_2 layer. Scanning electrochemical microscopy showed a decrease in corrosion currents with resistance to pitting corrosion attack on the WE43 sample in the presence of HQ after an exposure of 48 h. The formation of protective MgQ_2 layer on the WE43 samples was confirmed by XRD, XPS, and fluorescence microscopy analyses. The present study brings out the importance of metal-complexing organic agent, hydroxyquinoline, in initial acceleration and subsequent prevention of corrosion.

Acknowledgments

The authors thank the Materials Research Facility (MRF) for providing access to the microscopy, XRD, and XPS facilities. The authors thank Advanced Materials and Manufacturing Processes Institute (AMMPI) for the access to scanning electrochemical microscopic analysis.

References

1. A. Atrens, G.L. Song, M. Liu, Z. Shi, F. Cao, and M.S. Dargusch, Review of Recent Developments in the Field of Magnesium Corrosion, *Adv. Eng. Mater.*, 2015, **17**, p 400–453
2. G. Song and A. Atrens, Understanding Magnesium Corrosion—A Framework for Improved Alloy Performance, *Adv. Eng. Mater.*, 2003, **5**, p 837–858
3. E. Ghali, W. Dietzel, and K.U. Kainer, General and Localized Corrosion of Magnesium Alloys: A Critical Review, *J. Mater. Eng. Perform.*, 2004, **13**, p 7–23
4. M. Esmaily, J.E. Svensson, S. Fajardo, N. Birbilis, G.S. Frankel, S. Virtanen, R. Arrabal, S. Thomas, and L.G. Johansson, Fundamentals and Advances in Magnesium Alloy Corrosion, *Prog. Mater Sci.*, 2017, **89**, p 92–193
5. G. Williams, H.N. McMurray, and R. Grace, Inhibition of Magnesium Localised Corrosion in Chloride Containing Electrolyte, *Electrochim. Acta*, 2010, **55**, p 7824–7833
6. N.H. Helal and W.A. Badawy, Environmentally Safe Corrosion Inhibition of Mg-Al-Zn Alloy in Chloride Free Neutral Solutions by Amino Acids, *Electrochim. Acta*, 2011, **56**, p 6581–6587
7. O.V. Karavai, A.C. Bastos, M.L. Zheludkevich, M.G. Taryba, S.V. Lamaka, and M.G.S. Ferreira, Localized Electrochemical Study of Corrosion Inhibition in Microdefects on Coated AZ31 Magnesium Alloy, *Electrochim. Acta*, 2010, **55**, p 5401–5406
8. I.A. Kartsonakis, S.G. Stanciu, A.A. Matei, E.K. Karaxi, R. Hristu, A. Karantonis, and C.A. Charitidis, Evaluation of the Protective Ability of Typical Corrosion Inhibitors for Magnesium Alloys Towards the Mg ZK30 Variant, *Corrs. Sci.*, 2015, **100**, p 194–208
9. D. Huang, J. Hu, G.L. Song, and X. Guo, Inhibition Effect of Inorganic and Organic Inhibitors on the Corrosion of Mg-10Gd-3Y-0.5Zr Alloy in an Ethylene Glycol Solution at Ambient and Elevated Temperatures, *Electrochim. Acta*, 2011, **56**, p 10166–10178
10. D. Seifzadeh, H. Basharnavaz, and A. Bezaatpour, A Schiff Base Compound as Effective Corrosion Inhibitor for Magnesium in Acidic Media, *Mater. Chem. Phys.*, 2013, **138**, p 794–802
11. T. Ishizaki, J. Hieda, N. Saito, N. Saito, and O. Takai, Corrosion Resistance and Chemical Stability of Super-Hydrophobic Film Deposited on Magnesium Alloy AZ31 by Microwave Plasma-Enhanced Chemical Vapor Deposition, *Electrochim. Acta*, 2010, **55**, p 7094–7101
12. H. Gao, Q. Li, Y. Dai, F. Luo, and H.X. Zhang, High Efficiency Corrosion Inhibitor 8-Hydroxyquinoline and Its Synergistic Effect with Sodium Dodecylbenzenesulphonate on AZ91D Magnesium Alloy, *Corros. Sci.*, 2010, **52**, p 1603–1609
13. Q. Zong, L. Wang, W. Sun, and G. Liu, Active Deposition of bis (8-Hydroxyquinoline) Magnesium Coating for Enhanced Corrosion Resistance of AZ91D Alloy, *Corros. Sci.*, 2014, **89**, p 127–136
14. S. Shen, Y. Zuo, and X. Zhao, The Effects of 8-Hydroxyquinoline on Corrosion Performance of a Mg-Rich Coating on AZ91D Magnesium Alloy, *Corros. Sci.*, 2013, **76**, p 275–283
15. J. Hu, D. Zeng, Z. Zhang, T. Shi, G.L. Song, and X. Guo, 2-Hydroxy-4-Methoxy-Acetophenone as an Environment-Friendly Corrosion Inhibitor for AZ91D Magnesium Alloy, *Corros. Sci.*, 2013, **74**, p 35–43
16. J. Hu, D. Huang, G.L. Song, and X. Guo, The Synergistic Inhibition Effect of Organic Silicate and Inorganic Zn Salt on Corrosion of Mg-10Gd-3Y Magnesium Alloy, *Corros. Sci.*, 2011, **53**, p 4093–4101
17. L. Yang, Y. Li, B. Qian, and B. Hou, Polyaspartic Acid as a Corrosion Inhibitor for WE43 Magnesium Alloy, *J. Mag. Alloys*, 2015, **3**, p 47–51
18. M. Borrel and R.A. Paris, Precipitation Domains and Solubility Products of Some Oxinates and Methyloxinates, *Anal. Chim. Acta*, 1952, **6**, p 389–399 (in French)
19. S.H. Salleh, S. Thomas, J.A. Yuwono, K. Venkatesan, and N. Birbilis, Enhanced Hydrogen Evolution on $Mg(OH)_2$ Covered Mg Surfaces, *Electrochim. Acta*, 2015, **161**, p 144–152
20. S.K. Panigrahi, W. Yuan, R.S. Mishra, R. Delorme, B. Davis, R.A. Howell, and K. Cho, A Study on the Combined Effect of Forging and Aging in Mg-Y-RE Alloy, *Mater. Sci. Eng., A*, 2011, **530**, p 28–35
21. R. Pinto, M.G.S. Ferreira, M.J. Carmezim, and M.F. Montemor, Passive Behavior of Magnesium Alloys (Mg-Zr) Containing Rare-Earth Elements in Alkaline Media, *Electrochim. Acta*, 2010, **55**, p 2482–2489
22. H. Ardelean, A. Seyeux, S. Zanna, F. Prima, I. Frateur, and P. Marcus, Corrosion Processes of Mg-Y-Nd-Zr Alloys in Na_2SO_4 Electrolyte, *Corros. Sci.*, 2013, **73**, p 196–207
23. S.V. Lamaka, B. Vaghefinazari, D. Mei, R.P. Petrauskas, D. Hoche, and M.L. Zheludkevich, Comprehensive Screening of Mg Corrosion Inhibitors, *Corros. Sci.*, 2017, **128**, p 224–240
24. A. Atrens and W. Dietzel, The Negative Difference Effect and Unipositive Mg+, *Adv. Eng. Mater.*, 2007, **9**, p 292–297
25. S. Bender, J. Goellner, A. Heyn, and S. Schmigalla, A New Theory for the Negative Difference Effect in Magnesium Corrosion, *Mater. Corros.*, 2012, **63**, p 707–712
26. K.C. Tekin, U. Malayoglu, and S. Shrestha, Electrochemical Behavior of Plasma Electrolytic Oxide Coatings on Rare Earth Element Containing Mg Alloys, *Surf. Coat. Technol.*, 2013, **236**, p 540–549
27. W. Jin, G. Wu, H. Feng, W. Wang, X. Zhang, and P.K. Chu, Improvement of Corrosion Resistance and Biocompatibility of Rare-Earth WE43 Magnesium Alloy by Neodymium Self-Ion Implantation, *Corros. Sci.*, 2015, **94**, p 142–155
28. A.D. King, N. Birbilis, and J.R. Scully, Accurate Electrochemical Measurement of Magnesium Corrosion Rates; A Combined Impedance, Mass-Loss and Hydrogen Collection Study, *Electrochim. Acta*, 2014, **121**, p 394–406
29. V. Shkirskiy, A.D. King, O. Gharbi, P. Volovitch, J.R. Scully, K. Ogle, and N. Birbilis, Revisiting the Electrochemical impedance Spectroscopy of Magnesium with Online Inductively Coupled Plasma Atomic Emission Spectroscopy, *ChemPhysChem*, 2015, **16**, p 536–539
30. G.R. Argade, K. Kandasamy, S.K. Panigrahi, and R.S. Mishra, Corrosion Behavior of a Friction Stir Processed Rare-Earth Added Magnesium Alloy, *Corros. Sci.*, 2012, **58**, p 321–326
31. S. Thomas, J. Izquierdo, N. Birbilis, and R.M. Souto, Possibilities and Limitations of Scanning Electrochemical Microscopy of Mg and Mg Alloys, *Corrosion*, 2014, **71**, p 171–183
32. J.R. Lakowicz, *Principles of Fluorescence Spectroscopy*, 3rd ed., Springer, Singapore, 2006